Analysis of a bimetallic slab in non-isothermal flow

E Turan* and **A Ecder**
Department of Mechanical Engineering, Bogazici University, Istanbul, Turkey

The manuscript was received on 2 December 2009 and was accepted after revision for publication on 5 August 2010.

DOI: 10.1243/09544062JMES2135

Abstract: The main object of this study is to investigate a fluid–structure interaction problem using Newton–Krylov techniques. As a test problem, a bimetallic slab exposed to a non-isothermal flow field is selected. If the metals on the body have different coefficients of thermal expansion, then the structure deflects in the case of a temperature change. In this study, natural convection is the reason for the temperature gradient on the slab. Solution of incompressible Navier–Stokes equations are weakly coupled with the linearized quasi-static thermoelasticity problem. The Stream function–vorticity approach is used to analyse the governing equations of the flow problem and finite differences are used for discretization. The finite-element method is preferred to solve the deflection of the solid which is modelled with plane strain assumption. Matrix-free methodology is utilized in the Newton–Krylov solver. The inexact Newton method is employed along with preconditioned Generalized Minimum RESidual as the linear solver. Domain decomposition is utilized both to ease the solution of the deformed flow geometry and to separate both physics. Several computations are performed for various Rayleigh numbers and various results are presented.

Keywords: Newton–Krylov, domain decomposition, matrix-free, fluid–structure interaction, free convection, thermoelasticity

1 INTRODUCTION

In recent years, scientists worked with reduced models to analyse complex problems by carrying out several simplifying assumptions to overcome the difficulties of the actual cases. Although, at first sight, such an approach fitted perfectly to numerous classical problems, there is a bunch of observations that cannot be explained with single physics. Flutter, for instance, is unstable response of structures because of the aerodynamic forces on them and could only be realized using the aeroelasticity [**1**]. In nature, most of the real-life incidents definitely involve more than one physics, like combustion, aeroacoustics, fluid–structure interactions (FSIs) and many others. Since there is a need to perform multi-physics analysis, there is also a need for computational frameworks that handle different physics at the same time. Hence, the main object of this study is to contribute to the field with an analysis of an FSI problem while using Newton–Krylov techniques.

When Newton–Krylov techniques are used, outer iterations of the non-linear equations are performed with the Newton's method while the inner iterations to solve the linearized system are handled with Krylov subspace methods, such as Generalized Minimum RESidual (GMRES) [**2**] or BiCGStab [**3**]. The main advantage of Krylov subspace methods is that the Jacobian is not needed explicitly (except in preconditioning); the result of a matrix–vector product suffices for the computations. To compute the outcome of the multiplication, directional differencing is used at which the multiplier vector is perturbed by a parameter and applied on the non-linear system. This approach is called the matrix-free methodology and the selection of the perturbation parameter is crucial for the accuracy of the calculations. In Newton–Krylov techniques, it is also important to avoid excessive solution of the Jacobian system and an inexact Newton method should be used [**4**]. Many studies are carried out on Newton–Krylov techniques. Brown and Saad [**5**] investigated damping strategies for globalized solution of non-linear systems and applied Newton–GMRES method on a lid-driven cavity problem. Gropp *et al.* [**6**] explained the use of implicit solution techniques and made remarks for the improvement of the convergence of Newton's method.

**Corresponding author: Department of Mechanical Engineering, Bogazici University, Istanbul 34342, Turkey.*
email: turane@gmail.com

More recently, Pawlowski *et al*. [**7**] applied same ideas on challenging fluid mechanics problems including one natural convection problem.

As an FSI problem, flow around a bimetallic slab is examined. A bimetallic slab is composed of two metals each having a different coefficient of thermal expansion. When the temperature of the solid is changed from its initial state, for example, when the temperature rises, the solid deflects. The reason for the deflection is that the two parts of the structure elongate in different amounts; however, since they are bonded to each other, bending occurs instead of a pure elongation. The mechanics of a bimetallic solid is thoroughly investigated by Timoshenko [**8**]. The monograph of reference [**9**] also gives valuable information on thermal stresses. The aim of this study is to deflect the structure with a non-uniform temperature field rather a constant temperature difference. This field is generated by the non-isothermal flow around the body. The fluid problem is selected as a natural convection problem which is more challenging and interesting to investigate with Newton–Krylov techniques. Natural convection flow in a square cavity is a frequently investigated problem [**10–12**]; however, a study on the same geometry is seldom performed. Nonetheless, Shi and Khodadadi [**13**] investigated flow around a thin fin with varying length located in different positions in a square cavity. Semi-implicit method for pressure linked equations (SIMPLE) is used in conjunction with the quadratic upstream interpolation for convective kinematics (QUICK) scheme to resolve the flow field up to $Ra = 10^7$. Bilgen [**14**] also investigated a similar problem where a thin fin is attached to the vertical wall. The analysis is performed for different fin locations and lengths on various Rayleigh numbers using the SIMPLE revised algorithm. In this study, in contrast to [**13**], the temperature distribution within the fin is taken into consideration, as well.

In this study, an alternating domain decomposition analysis is performed, which is originally investigated by Schwarz [**15**]. By means of overlapping domains, the changes in the fluid boundaries are captured and examined in simple geometries. The overall analysis is based on the interaction of a free convection flow around a bimetallic structure. Non-isothermal flow field around the body deforms the geometry because of the deflection of a two-layered slab which in turn modifies the domain of the fluid region, as well. Momentum and energy equations are coupled with each other through the buoyancy term (i.e. gravity). Although this work is limited with a steady-state solution, several iterations are performed between solid and fluid problems. In section 2, the equations of the model problem is given and the details of the coupling algorithm is explained. In section 3, numerical methods are covered. Section 4 is devoted for the result of the study. Section 5 summarizes the work done and suggests ideas for future work.

2 DESCRIPTION OF THE PROBLEM

The problem consists of two physics: fluid and solid domains. For the sake of the analysis, the equations of both physics should be presented. Governing equations of fluid mechanics are the Navier–Stokes equations. The general form of incompressible Navier–Stokes equations is given in equations (1) to (3) [**16**] where u denotes the velocity field, p is the pressure, T is the temperature, and ρ, μ, k, c_p, denote the density, dynamic viscosity, conductivity, and specific heat, respectively. Equation (1) is the mass conservation, whereas equation (2) is the momentum equations for each velocity component and equation (3) is the energy equation. For a forced convection problem, the energy and momentum equations are decoupled. Once the flow field is determined, the temperature field can easily be extracted

$$\nabla \cdot \boldsymbol{u} = 0 \tag{1}$$

$$\rho \mathbf{u} \cdot \nabla \boldsymbol{u} = -\nabla p + \mu \nabla^2 \boldsymbol{u} + \rho \boldsymbol{f} \tag{2}$$

$$\rho c_p \boldsymbol{u} \cdot \nabla T = k \nabla^2 T \tag{3}$$

On the other hand, in a free convection problem, the variation of the density cannot be ignored. The fluid motion in natural convection is driven by the buoyancy. Although the density is not constant all over the domain, an assumption on the variation of the density can be made through the Boussinesq approximation [**16**] given in equation (4), β being the thermal expansion coefficient of the fluid and subscript r denoting reference values. With the introduction of Boussinesq assumption, density is taken constant throughout the entire equation set except the body forces

$$(\rho - \rho_\mathrm{r}) \approx \rho_\mathrm{r} \beta (T - T_\mathrm{r}) \tag{4}$$

Use of this approximation couples the momentum and energy equations, so two velocities (u, v), pressure (p), and the temperature (T), should be solved at once. However, instead of solving these primary unknowns, one could use the stream function (ψ) – vorticity (Ω) formulation to determine the flow field. The advantage of following this methodology rather than the primitive variables (u, v, p, T) is that complications related to the treatment of the pressure can be eliminated, and in two-dimensional (2D) coordinate systems, this approach is computationally more efficient because of reduced number of unknowns. The non-dimensional form of the equations in both Cartesian and polar coordinates are given in equations (5) to (10). The polar form is also introduced since it will be used in the

deflected parts of the fluid domain

$$\frac{\partial^2\psi}{\partial x^2}+\frac{\partial^2\psi}{\partial y^2}=-\Omega \tag{5}$$

$$Pr\left[\frac{\partial^2\Omega}{\partial x^2}+\frac{\partial^2\Omega}{\partial y^2}\right]+RaPr\frac{\partial T}{\partial x}-\left[\frac{\partial\psi}{\partial y}\frac{\partial\Omega}{\partial x}-\frac{\partial\psi}{\partial x}\frac{\partial\Omega}{\partial y}\right]=0 \tag{6}$$

$$\left[\frac{\partial^2 T}{\partial x^2}+\frac{\partial^2 T}{\partial y^2}\right]-\left[\frac{\partial\psi}{\partial y}\frac{\partial T}{\partial x}-\frac{\partial\psi}{\partial x}\frac{\partial T}{\partial y}\right]=0 \tag{7}$$

$$\frac{\partial^2\psi}{\partial r^2}+\frac{1}{r}\frac{\partial\psi}{\partial r}+\frac{1}{r^2}\frac{\partial^2\psi}{\partial\theta^2}=-\Omega \tag{8}$$

$$Pr\left[\frac{\partial^2\Omega}{\partial r^2}+\frac{1}{r}\frac{\partial\Omega}{\partial r}+\frac{1}{r^2}\frac{\partial^2\Omega}{\partial\theta^2}\right]-\left[\frac{\partial\psi}{\partial\theta}\frac{\partial\Omega}{\partial r}-\frac{\partial\Omega}{\partial\theta}\frac{\partial\psi}{\partial r}\right]+RaPr\left[\frac{1}{r}\frac{\partial T}{\partial\theta}\cos(\theta)+\frac{\partial T}{\partial r}\sin(\theta)\right]=0 \tag{9}$$

$$\left[\frac{\partial^2 T}{\partial r^2}+\frac{1}{r}\frac{\partial T}{\partial r}+\frac{1}{r^2}\frac{\partial^2 T}{\partial\theta^2}\right]-\frac{1}{r}\left[\frac{\partial\psi}{\partial\theta}\frac{\partial T}{\partial r}-\frac{\partial T}{\partial\theta}\frac{\partial\psi}{\partial r}\right]=0 \tag{10}$$

The most important parameter in these equations is the Rayleigh number, *Ra*. The problem gets harder to analyse as *Ra* number increases. The reason for this complication is that the non-linearity increases as the convective terms dominate the flow conditions. Prandtl number, *Pr*, is the other physical parameter and compares the velocity and thermal boundary layers; however, in the present study it is taken as unity

$$Ra=\frac{g\beta H^3(T_0-T_r)}{\alpha\nu},\quad Pr=\frac{\nu}{\alpha} \tag{11}$$

Boundary condition for stream function, ψ, is set to zero; however, for vorticity, Ω, equation (12) should be implemented where subscript wall denotes a node on the wall and wall -1 denotes an interior node in the vicinity of the wall

$$\Omega_{\text{wall}}=\frac{2(\psi_{\text{wall}}-\psi_{\text{wall}-1})}{\Delta n^2} \tag{12}$$

Bottom and top walls are assumed to be insulated and therefore homogeneous Neumann boundary conditions are implemented for the dimensionless temperature as seen in Fig. 1. Temperature of the left wall is unity ($T=1$) and the right wall is kept as zero ($T=0$). Temperature boundary conditions on the metallic slab are complicated. At the first solve of the convection problem, the surface of the solid is also taken as zero. Later, the temperature values are determined by the coupling algorithm. Before giving the details of the implementation, the thermoelastic problem should also be presented.

Second physics of the problem is the solid part which is a bimetallic slab composed of two different metals. Main feature of a bimetallic slab is the difference between the coefficient of thermal expansion, α of two materials. In the presence of a temperature gradient, the metal will bend since the elongations of the layers will be in different amounts. Heat transfer and elasticity are coupled with each other; however, with a linearized assumption, both fields can be decoupled and the deflection and the temperature distribution can be solved with iterations between each system. This model problem is in two dimensions (infinitely long in third dimension); as a result, a plane-strain assumption is appropriate for solving the displacement field. Equations (13) and (14) state the equilibrium and equation (15) gives the relation between the strains and the displacements [**17**]. u and v in equation (15) should not be confused with the velocity components in Navier–Stokes equations. Since the fluid flow is now analysed with stream function (ψ) and vorticity (ω) formulation, u and v throughout this study will point the displacements in x- and y-directions, respectively

$$\frac{\partial\sigma_x}{\partial x}+\frac{\partial\tau_{xy}}{\partial y}=-f_x \tag{13}$$

$$\frac{\partial\tau_{xy}}{\partial x}+\frac{\partial\sigma_y}{\partial y}=-f_y \tag{14}$$

$$\begin{Bmatrix}\varepsilon_x\\ \varepsilon_y\\ \gamma_{xy}\end{Bmatrix}=\begin{bmatrix}\frac{\partial}{\partial x} & 0\\ 0 & \frac{\partial}{\partial y}\\ \frac{\partial}{\partial y} & \frac{\partial}{\partial x}\end{bmatrix}\begin{Bmatrix}u\\ v\end{Bmatrix} \tag{15}$$

In order to perform a displacement-based finite-element analysis, the constitutive equation should also be given. For an isotropic homogeneous material the constitutive equation, $\sigma=\mathbf{D}\varepsilon$, is given in equation (16) where the material stiffness matrix, **D**, is valid for plane strain [**18**]

$$\begin{Bmatrix}\sigma_x\\ \sigma_y\\ \tau_{xy}\end{Bmatrix}=\frac{E(1-\nu)}{(1+\nu)(1-2\nu)}\times\begin{bmatrix}1 & \frac{\nu}{1-\nu} & 0\\ \frac{\nu}{1-\nu} & 1 & 0\\ 0 & 0 & \frac{1-2\nu}{2(1-\nu)}\end{bmatrix}\begin{Bmatrix}\varepsilon_x\\ \varepsilon_y\\ \gamma_{xy}\end{Bmatrix} \tag{16}$$

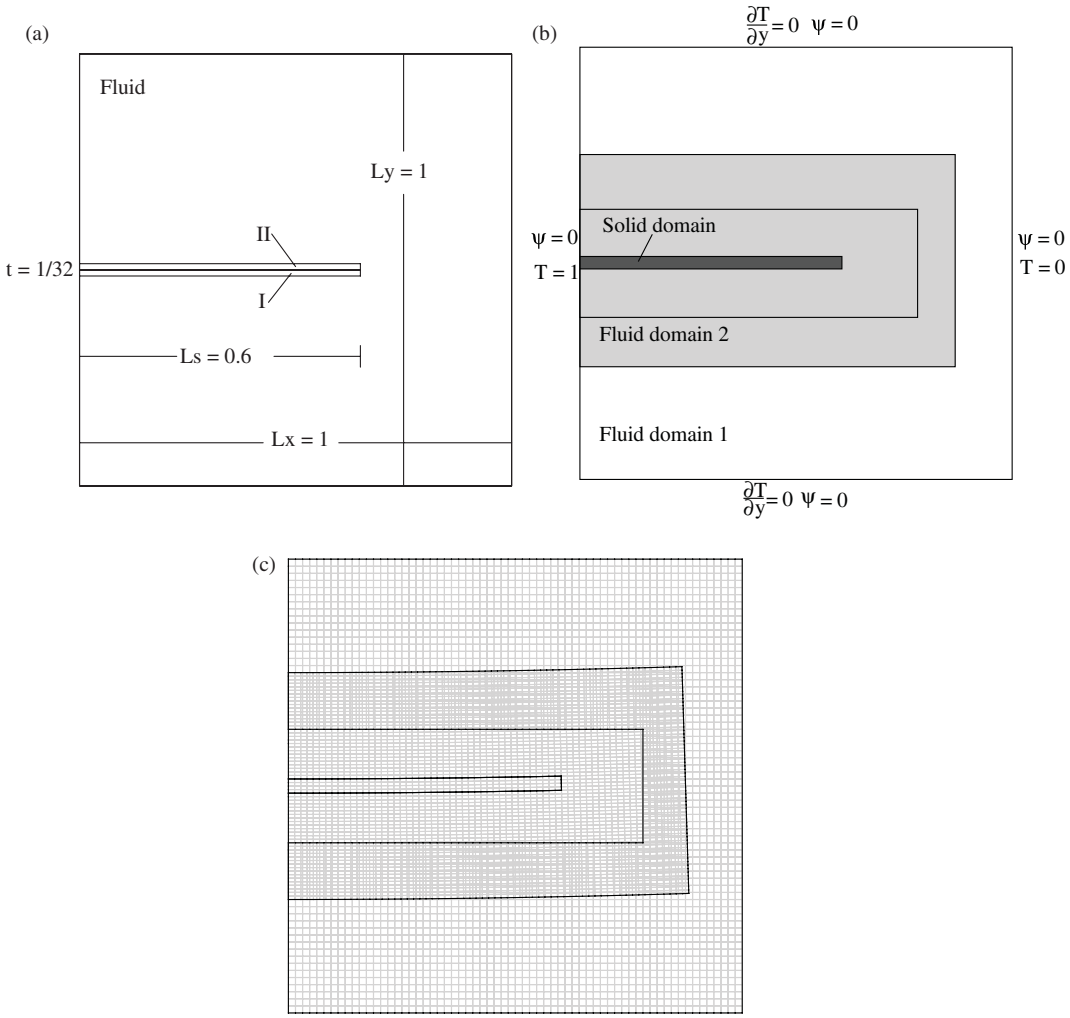

Fig. 1 Description of the geometry and the boundary conditions and mesh of the domains

In order to calculate the thermal stresses, the constitutive relation should be modified as $\sigma = \mathbf{D}(\epsilon - \epsilon_{\mathrm{T}})$, and the effect of thermal expansion through the thermal strain, ϵ_{T}, should be included. For plain-strain problems, thermal strain is defined as in equation (17) at which α_{s} is the coefficient of thermal expansion and ΔT is the temperature difference [**19**] . It can be seen that only normal strain components are affected by the change in the temperature

$$\varepsilon_{\mathrm{T}} = (1+\nu)\begin{Bmatrix} \alpha_{\mathrm{s}}\Delta T \\ \alpha_{\mathrm{s}}\Delta T \\ 0 \end{Bmatrix} \tag{17}$$

Although the governing equations of the fluid model are discretized with finite differences, the displacements are calculated with finite elements using bilinear quadrilaterals. The equations that lead a system like $\mathbf{K}\boldsymbol{u} = \mathbf{F}$ are given in equations (18) and (19)

$$\mathbf{K} = \int_A \mathbf{B}^{\mathrm{T}}\mathbf{D}\mathbf{B}\,\mathrm{d}A \tag{18}$$

$$\mathbf{F} = \int_A \mathbf{B}^{\mathrm{T}}\mathbf{D}\varepsilon_{\mathrm{T}}\,\mathrm{d}A \tag{19}$$

with

$$\mathbf{N} = \begin{bmatrix} N_1 & 0 & N_2 & 0 & N_3 & 0 & N_4 & 0 \\ 0 & N_1 & 0 & N_2 & 0 & N_3 & 0 & N_4 \end{bmatrix},$$

$$\mathbf{B} = \begin{bmatrix} \dfrac{\partial}{\partial x} & 0 \\ 0 & \dfrac{\partial}{\partial y} \\ \dfrac{\partial}{\partial y} & \dfrac{\partial}{\partial x} \end{bmatrix} \times \mathbf{N} \tag{20}$$

where N_i is the shape function of the ith node, and ε_{T} is the thermal strain [**18**]. The solid is attached to the left side of the wall from its right end and free on the other end. Both degrees of freedom, u and v, are kept zero.

Because of the deformed geometry, it is also convenient to solve the heat conduction on the solid with

finite elements. The procedure is similar to the elastic case, $\mathbf{K}_C\mathbf{T} = \mathbf{F}_C$ can be calculated from equations (21) and (22), where subscript C denotes a conduction problem and q is the heat flux, and k_{xx}, k_{yy} are thermal conductivities in x and y co-ordinates, respectively

$$\mathbf{K}_C = \int_A \mathbf{B}_C^T \mathbf{D}_C \mathbf{B}_C \, dA \tag{21}$$

$$\mathbf{F}_C = -\int_S q\mathbf{N}_C^T \, dS \tag{22}$$

with

$$\mathbf{B}_C = \begin{bmatrix} \frac{\partial N_1}{\partial x} & \frac{\partial N_2}{\partial x} & \frac{\partial N_3}{\partial x} & \frac{\partial N_4}{\partial x} \\ \frac{\partial N_1}{\partial y} & \frac{\partial N_2}{\partial y} & \frac{\partial N_3}{\partial y} & \frac{\partial N_4}{\partial y} \end{bmatrix},$$

$$\mathbf{D}_C = \begin{bmatrix} k_{xx} & 0 \\ 0 & k_{yy} \end{bmatrix}, \quad \mathbf{N}_C^T = \begin{bmatrix} N_1 \\ N_2 \\ N_3 \\ N_4 \end{bmatrix} \tag{23}$$

2.1 Coupling procedure

In this study, a partitioned analysis [**20**] is performed and there is a two-way weak coupling between the physics. On the other hand, the thermoelastic coupling between the energy and elasticity problems on the slab is a one-way coupling: The temperature distribution is calculated on the structure and then the deformation is calculated via thermal loads on the body by solving the displacement field. Later, instead of updating the temperature profile for the deflected geometry, the computation continues with a recalculation of the flow field at which the temperature values on the nodes of the deformed solid is applied on the inner domain of the flow field for equation (10). The coupling procedure is summarized in Fig. 2. Although thermoelasticity is non-linear in a general sense because of the thermodynamic considerations [**21**], the analysis followed in this study performed well because the deformations stay in the linear elastic region and the problem is treated quasi-static because the computations are handled in an iterative fashion by visiting both physics, and final convergence is needed only at the end.

Focusing on the multi-physics, the coupling between two physics is mainly established with heat flow. Assuming an initial temperature for the slab, the free convection problem is solved with the non-homogeneous Dirichlet boundary condition where first solve is attempted with the initial temperature as the boundary condition. Temperature distribution inside the structure is computed with non-homogeneous Neumann boundary conditions calculated within the values of the fluid domain. Thereafter, the temperature values on the surface of

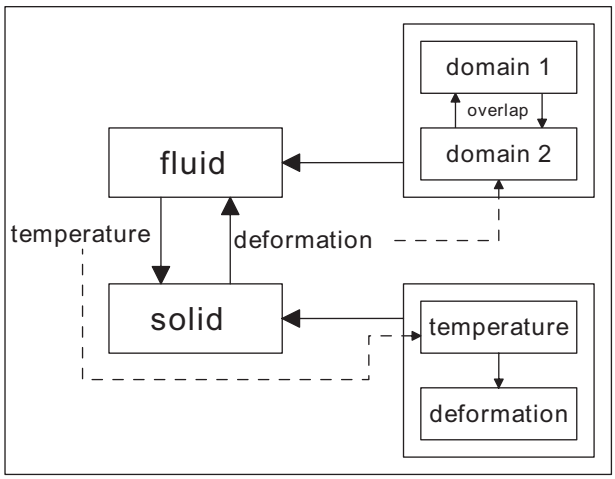

Fig. 2 Solution algorithm

the solid body are used as the boundary condition of the flow problem. Once a temperature distribution on the structure is calculated and the deformation is determined, this temperature field is treated as the initial state for the next computations.

When the solid deforms, the boundaries of the flow should be modified accordingly. This can normally be accomplished with a regeneration of the mesh after each deflection. Instead of this approach, a method based on domain decomposition is followed. Basically, the domain of the fluid is divided into two overlapping, non-conforming grids as observed in Fig. 1. Outer grid preserves its shape while the inner adjusts itself with the deflection of the solid part. Iterations between domains will continue until convergence is achieved. Two remarks should be stated before proceeding with the next section. The pressure on the solid as a result of the fluid is ignored mainly because the pressure is not significant compared to a forced convection problem. Only thermal conditions are effective on the solid. It should also be mentioned that an average radius of curvature is to be found since the deformed subdomain is assumed to be in polar co-ordinates. To facilitate the new geometry, an average radius of curvature must be calculated with a least-squares approximation. This way, the new geometry can be constructed with the average curvature. If some portion of the solid deforms unexpectedly more than the rest, then the extra deflection can be damped with this strategy. In this study, the problems regarding the advection of the deforming mesh are not addressed mainly because a steady-state solution is sought, and intermediate problems are treated as being steps towards the steady physics.

3 NUMERICAL METHODS

In this study, several methods are covered to solve the problem. Systems of nonlinear equations are solved

with Newton's method and linear problems are handled with GMRES, one of many Krylov solvers. The so-called Newton–Krylov methodology is improved with the matrix-free idea where the formation of the Jacobian is avoided. Additionally, domain decomposition is employed and particularly in two different ways. First, it is used to separate the physics of the problem into fluid and solid domains. Second, it is used to simplify the analysis of the fluid domains where the deformations are confined in a subdomain so that it is conformable with the solid domain.

3.1 Preconditioned Newton-GMRES method

Newton's method is frequently used to solve systems of non-linear equations, $\boldsymbol{f}$. In this method, computations start with an initial guess, $\boldsymbol{x}_0$, and the solution vector, $\boldsymbol{x}$, is updated after each iteration as in equation (24). GMRES [**2**] is a linear solver for non-symmetric matrices and employed for the solution of equation (25) where $J_{ij} = \partial f_i / \partial x_j$ is the Jacobian matrix. In this study, inexact Newton's method (equation (26)) [**4**] is also considered, so one can avoid finding too accurate updates for early iterations of the non-linear solution process. In these equations, λ is the damping parameter and η is the forcing term, both ranging in (0, 1]

$$\boldsymbol{x}_{k+1} = \boldsymbol{x}_k + \lambda \boldsymbol{p} \tag{24}$$

$$\mathbf{J}(\boldsymbol{x}_k)\boldsymbol{p} = -\boldsymbol{f}(\boldsymbol{x}_k) \tag{25}$$

$$\|\boldsymbol{f}(\boldsymbol{x}_k) + \mathbf{J}(\boldsymbol{x}_k)\boldsymbol{p}\| \leqslant \eta \|\boldsymbol{f}(\boldsymbol{x}_k)\| \tag{26}$$

While solving a linear system with GMRES, the matrix, $\mathbf{J}$, does not have to be explicitly evaluated. What is required is only a matrix–vector product which is also a vector. This property of GMRES is very useful in the analysis of the fluid flow with finite differences and the elastic deformation with finite elements. Finite differences are implemented with the matrix-free method to avoid the formation of the Jacobian matrix in equation (25). The multiplications are calculated with equation (27) at which the selection of parameter ε is crucial for the accuracy of the results [**5**, **6**, **22**]. In the author's computations, $\varepsilon = 1e-8$ gave good accuracy

$$\mathbf{J}\boldsymbol{v} \approx \frac{\boldsymbol{f}(\boldsymbol{x} + \varepsilon \boldsymbol{v}) - \boldsymbol{f}(\boldsymbol{x})}{\varepsilon} \tag{27}$$

In the finite-element method, global assembly of the stiffness matrix is avoided and the computations are done on an element-by-element (EBE) basis [**23**]. In the EBE approach, only local stiffness matrices are stored. If a multiplication is necessary, then the vector to be multiplied is operated only on the respective part of the local stiffness matrices. In this approach, storage considerations can be reduced significantly and the computations can be done in parallel processors.

When the Krylov solvers are in concern, it should be said that they perform poorly without a proper preconditioner. A compromise could be made when selecting the preconditioner. If a simple method such as Jacobi or Gauss–Seidel is selected, then the application of the preconditioner does not require that much of a computational power. On the other hand, the number of iterations necessary to fulfil the convergence criteria is still high. More advanced methods such as incomplete-LU decompositions with fill-ins, ILU(ℓ), are superior to those methods in terms of the iteration numbers; however, they require more space and time for the calculations. One should also pay attention to the matrix-free approach. Although the Jacobian matrix is not explicitly required in GMRES and in other Krylov solvers, an approximate matrix should be formed to perform the preconditioning. This matrix can either be formed from a low-order approximation of the problem or the Jacobian matrix might be calculated at the beginning of non-linear iterations and kept the same for several other updates. In this study, Jacobi preconditioner is picked as the preconditioner and it performed well for the range of Rayleigh numbers investigated.

3.2 Domain decomposition method

The domain decomposition method simplifies the analysis in several aspects. First, the number of the unknowns on each domain is smaller compared to the whole domain. On the other hand, when the total number of unknowns of all subdomains is in concern, the degree of freedom of this new problem exceeds the original full problem. However, the ability of using parallel processing in domain decomposition can resolve this problem. When small problems are realized in parallel, each subdomain can be analysed in different processors and with proper load-balancing, and inter-processor communications, the overall analysis can be optimized to succeed the full problem.

In this study, domain decomposition is used to fulfil another necessity that arises from the deformation of the solid boundary; regeneration of the grid. When the solid part deflects, the fluid domain should adapt to the change. This can be handled in a single domain either by grid generation all over the flow area or by moving the mesh in some amounts. Then again, the use of domain decomposition plays an important role and limits the generation of the grid only for the inner domain. In this way, several different cases can be analysed simultaneously by just varying the conditions only in the inner problem.

It should be said that, although an overlapping grids methodology is followed, the amount of overlap is changing as the metal deflects. This change also affects the convergence properties of the problem. When the geometry is deflected, the problem gets complicated,

so this overlap can be used to overcome the difficulties (or balance the computations) since it is known that the amount of overlap improves the domain decomposition analysis in the alternating Schwarz method [**24**]. After deflections of the domains, the data transfer between subdomains is achieved with bilinear interpolation. Calculated stream function, vorticity, and temperature values are applied directly regardless of the co-ordinate system.

Strikwerda and Scarbnick [**25**] proposed a strategy for interpolations between two different co-ordinate systems: during the interpolation, variables should be transformed first and then interpolation should be performed, rather than interpolation followed by transformation. In this study, velocities are not used so such a methodology can be ignored since the variables in this study, ψ, Ω, T, are all scalar. As a result, data interchange between domains is carried out by simple bilinear interpolations.

4 RESULTS AND DISCUSSION

In this study, several computations are performed for $10^0 \leqslant Ra \leqslant 10^6$. Pr is kept unity, except for the validation study. Newton's method is said to be converged for 10^{-5} order change on the initial residual. The maximum number of non-linear iterations is set as 20. If the domain solve is successful in 20 steps, then the solver passes to the other subdomain. GMRES(200) with Jacobi preconditioning is used as the linear solver. Iterations between fluid subdomains is stopped if 2-norm of the difference of two consecutive solves is less than 10^{-4}. It is observed that more strict tolerances do not affect the convergence of the domain decomposition method. For the coupling, the iterations between physics pronounced to be at the steady state if the change in the radius of convergence is less than 10^{-4}. A 65×65 grid is used in the flow problem and 176 elements are used for the thermoelastic problem. In section 4.1, the algorithm is tested against the study of reference [**14**]. In section 4.2, free convection results without deformations are presented. The last section is devoted for the results of the coupled problem.

4.1 Validation

In order to test the solution algorithm, several simulations are performed. Natural convection in a square cavity heated from one side and insulated from the top and bottom walls is a classic test problem which is investigated by several authors [**10–12**]. Validation of the solver is first performed for this model. Stream function and temperature fields for $Ra = 10^6$ are given in Fig. 3.

In Table 1, the result of Nusselt, Nu, number computations are presented. The average Nu number on the left wall of the cavity is compared against two reference studies and the results are within 1 per cent difference. The value of the local Nu number is calculated using three-point forward difference and the integration is performed using the Simpson's rule. Shi and Khodadadi [**13**] also provide several results for different fin geometries. As a test case, flow around a thin fin with half of the unit length located at $y = 0.5$ is investigated. The results are compared for the maximum absolute values of stream function, ψ. Temperature field for $Ra = 10^6$ is given in Fig. 4. In Fig. 4(b) two cases, w/ and w/o fin, are simulated and the results are in agreement with reference [**13**].

Finally, before solving the natural convection problem in the main geometry, another study is performed to compare the results with reference [**14**]. To do that, a thin strip is prepared with length 0.5 and

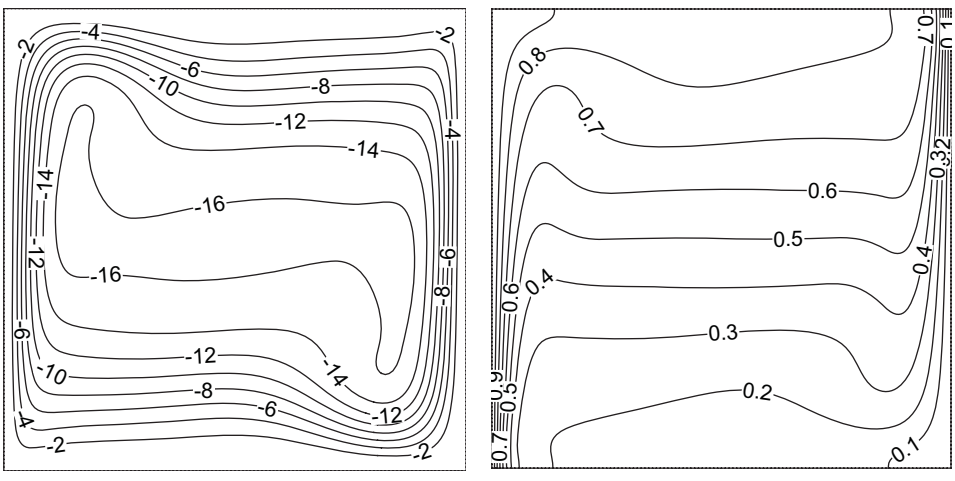

Fig. 3 Streamlines (a) and temperature field (b) for $Ra = 10^6$ and $Pr = 0.71$

Table 1 Average *Nu* on the left wall

Ra	10^4	10^5	10^6
de Vahl Davis [**10**]	2.238	4.509	8.817
Shi and Khodadadi [**13**]	2.247	4.532	8.893
Present study	2.251	4.53	8.85

thickness 0.01. As in the reference, the dimensionless conductivity of the fin is selected as 30 and *Pr* number is set to 0.7. The computations are performed for $Ra = 10^6$. Figure 5 demonstrates the comparison. In Fig. 5(a), the flow field of the current study is presented. In Fig. 5(b), the values are compared with reference [**14**] where the values agree with the findings of the reference study. Another important aspect of the comparison is that the result is taken from a domain decomposition solve. Similar to the main problem, also one interior and one outer domain are used. The plot reveals the fact that domain decomposition performs well.

4.2 Natural convection

In the first part, the problem is solved for a fixed radius of curvature, $\rho = 2.5$. Such a value is not encountered in the analysis of the FSI problem; however, it is given here to show that the solver is capable of handling large changes in the geometry. The results presented here are for $Ra = 10^4$ and $Ra = 10^5$. For this case, the dimensionless temperature value of the inner boundary of the polar domain is given as unity. Stream function contours as well as the temperature distribution for $Ra = 10^4$ and $Ra = 10^5$ are given in Figs 6 and 7, respectively. The boundaries of the subdomains are clearly visible. As one can notice, the solutions are in agreement in both domains and the contour lines pass smoothly from one domain to another. In Fig. 8, a typical non-linear convergence plot is shown for $Ra = 10^5$. After an initial increase in the non-linear norm, the residual starts to decrease at a steady rate and drops gradually in last steps, which is the property

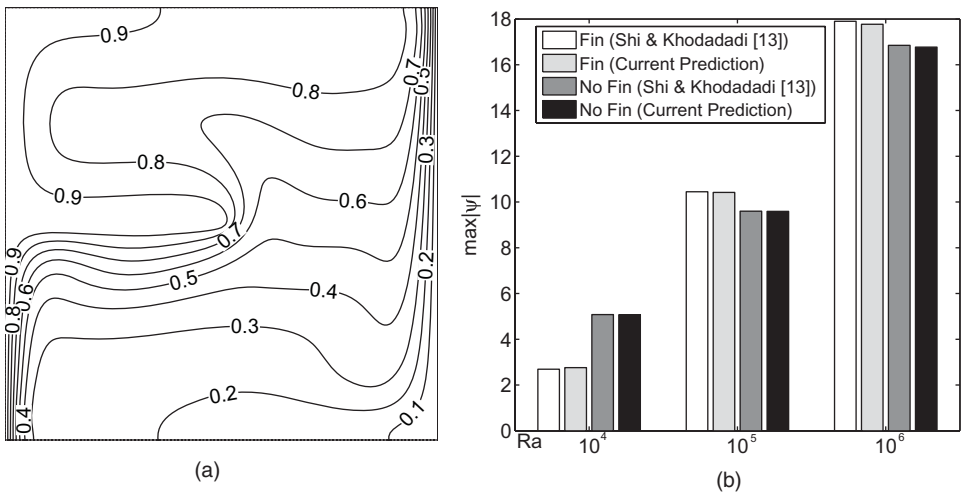

Fig. 4 (a) Temperature field and (b) max$|\psi|$

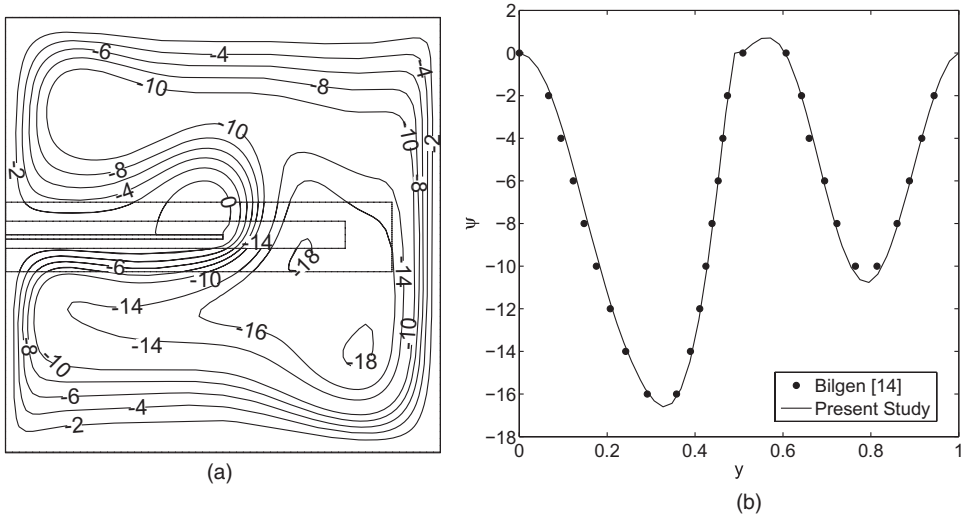

Fig. 5 Streamlines (a) comparison with reference [**14**] (b)

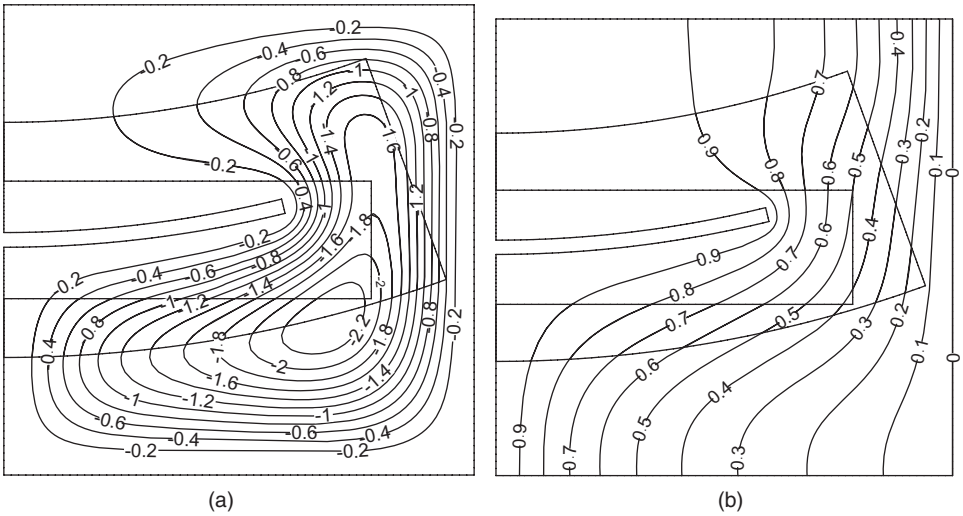

Fig. 6 Stream function (a) and temperature distribution (b) for $Ra = 10^4$ and $\rho = 2.5$

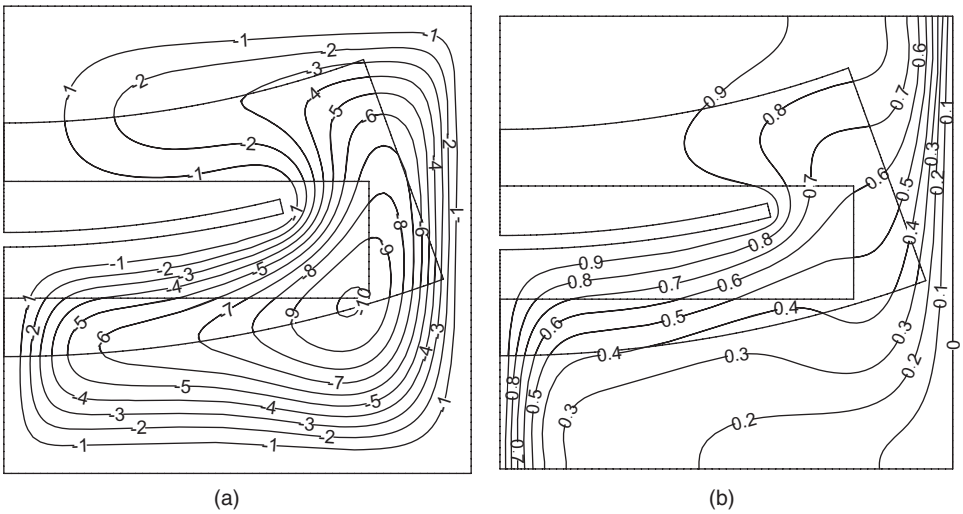

Fig. 7 Stream function (a) and temperature distribution (b) for $Ra = 10^5$ and $\rho = 2.5$

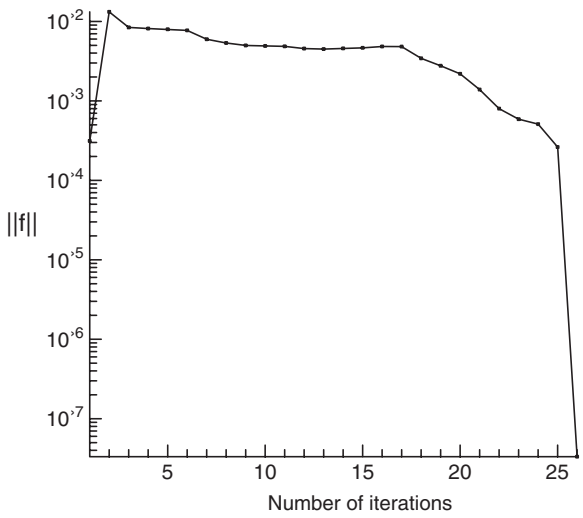

Fig. 8 Typical non-linear convergence history for $Ra = 10^5$

of Newton's method. In this part of the study, continuation over the parameter *Ra* is followed, so an improved initial guess is used for Newton's method. If an initial guess is not available, global convergence strategies like line search-backtracking can be employed [**5**]. In Fig. 9, the linear convergence of GMRES is presented. As observed from the figure, the performance of the Jacobi preconditioner is satisfactory.

4.3 Natural convection with deforming solid

In this section, the results of the main problem are given. For the solid part, the material properties given in Table 2 are used. As observed from the table, aluminium's thermal expansion coefficient is greater than that of steel's. Hence, as aluminium is on the bottom layer of the slab, a temperature rise within the body will deflect the solid in the positive y-direction. The equations in the solid part are solved dimensional; however, their values are kept the same of those

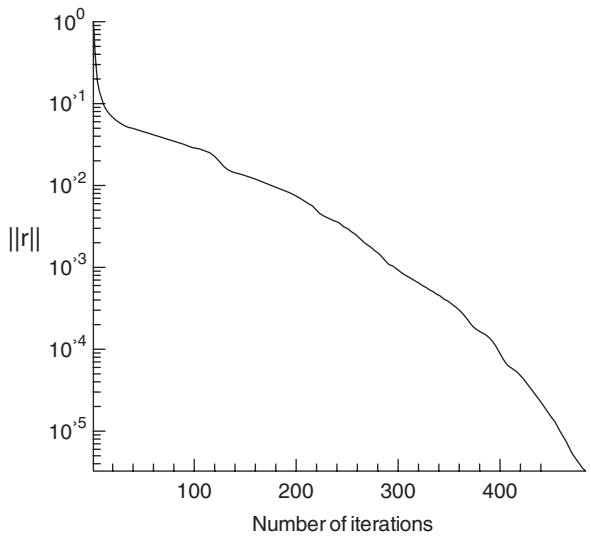

Fig. 9 Typical linear convergence history for GMRES at $Ra = 10^5$

Table 2 Material properties [**26**, **27**]

	Aluminium (I)	Steel (II)
Modulus of elasticity (E)	72 GPa	200 GPa
Poisson's ratio (ν)	0.35	0.28
Coefficient of thermal expansion (α_s)	23e-6 °C^{-1}	12e-6 °C^{-1}
Thermal conductivity (k)	237 W/(m K)	40 W/(m K)

of non-dimensional forms. On the other hand, the temperature is not taken equal. A temperature rise in the order of 1 would not generate enough deflection to deform the structure. That is why the values calculated in the flow field are scaled with 100. As a result, 100 times larger temperature difference is applied on the system, which is physically reasonable. The geometrical description of the problem is given in Fig. 1. Several computations are made for $Ra = 10^1, 10^2, 10^3, 10^4, 10^5, 10^6$. To be fair on comparisons, computations for all Ra numbers started from zero initial guesses.

In Fig. 10, temperature profiles for $Ra = 10^1, 10^2$ are shown. It is clear that both solutions are very similar. The radius of curvatures for all three cases are equal and read as 17.304. All three cases need 12 visits between the fluid and solid to converge. The total number of subdomain solves in the flow problem is 63 for $Ra = 10^1$ and 66 for $Ra = 10^2$. The results of $Ra = 10^3$ also resemble previous plots (Fig. 11). The radius of curvature is 17.304 and 12 iterations are needed for physics convergence, as well. Sixty seven total visits are observed for the solution of the free convection problem. Temperature profile of $Ra = 10^4$ is slightly different and convection starts to dominate the flow. The radius of curvature is not much different from the previous cases and equal to 17.503. Although, the total number of solves is equal to $Ra = 10^4$ with 67 visits, 13 iterations are needed between fluid and solid physics for a converged solution. $Ra = 10^5$ and $Ra = 10^6$ problems are numerically more challenging than the aforementioned cases because the non-linearity is increased and more domain solves are needed. Stream function contours are given in Fig. 12 and temperature distributions are given in Fig. 13. The radii of curvature are 19.372 and 28.868, respectively. $Ra = 10^5$ case converges in 18 physics iterations and performs 84 subdomain solves to get there. $Ra = 10^6$ converges in 40 iterations and needs 183 subdomain solves. In Fig. 14, the temperature distribution on the centre-line (i.e. on the interface of the slab for $Ra = 10^3, 10^4, 10^5, 10^6$ is given). As seen from the figure, the tip of the beam gets colder with increasing Ra number. This is expected because convection starts to dominate and cools the metal. This figure excludes temperature variation of smaller Ra numbers

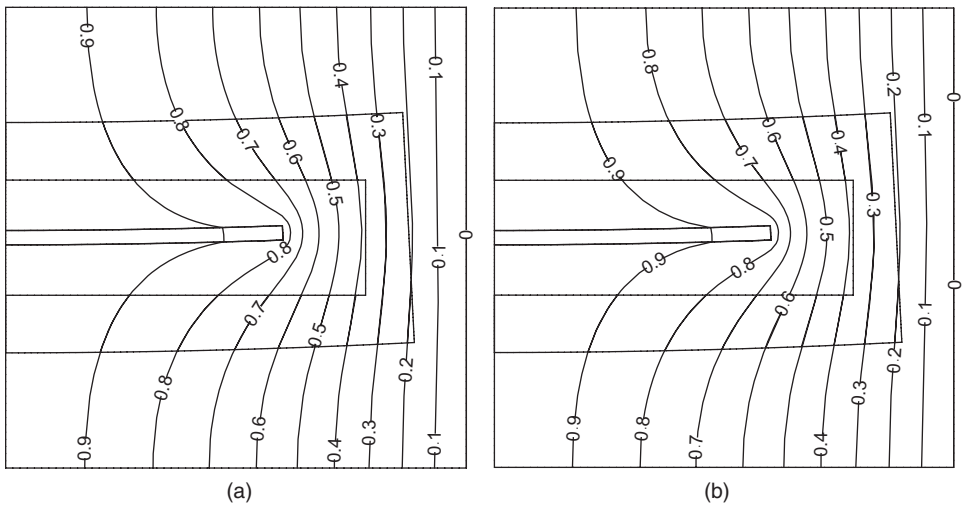

Fig. 10 Temperature distributions: (a) $Ra = 10^1$ and (b) $Ra = 10^2$

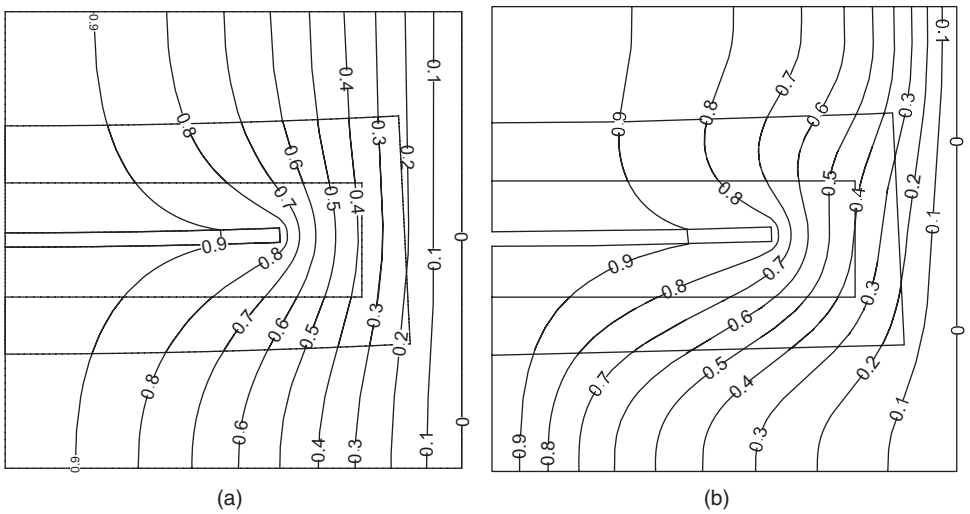

Fig. 11 Temperature distributions: (a) $Ra = 10^3$ and (b) $Ra = 10^4$

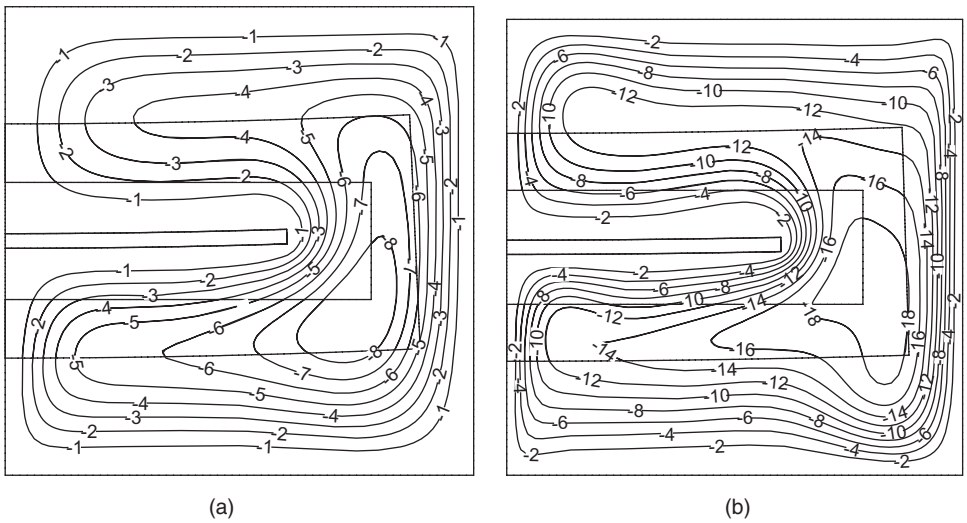

Fig. 12 Stream function contours: (a) $Ra = 10^5$ and (b) $Ra = 10^6$

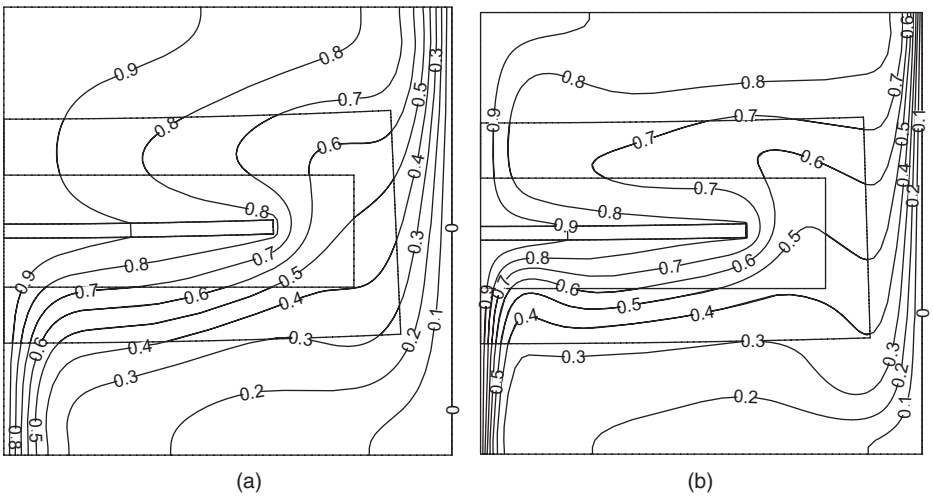

Fig. 13 Temperature distributions: (a) $Ra = 10^5$ and (b) $Ra = 10^6$

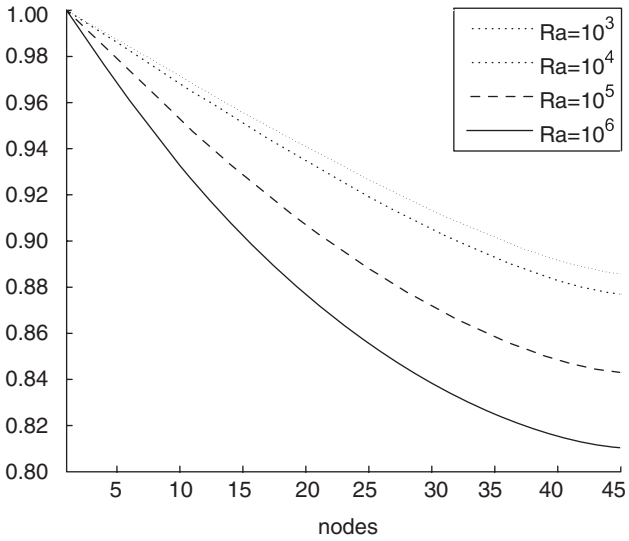

Fig. 14 Centre-line temperature profile

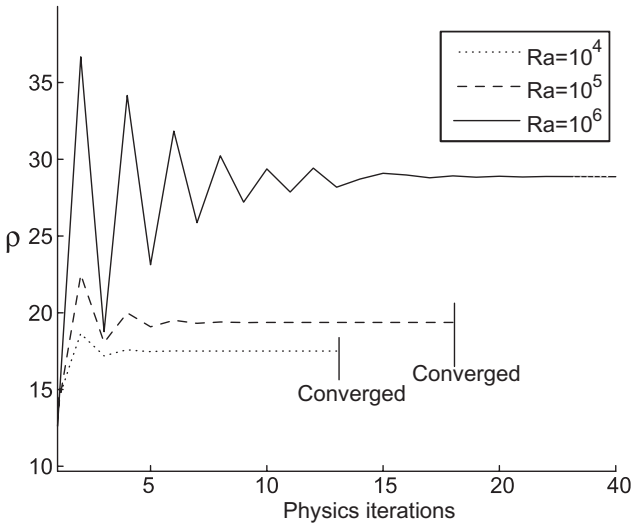

Fig. 16 Convergence of the radius of curvature

since they follow nearly the same profile of $Ra = 10^3$. Another outcome of this result is that temperature difference from the initial state decreases as *Ra* increases. That means the thermal load on the metal will be smaller for large *Ra* numbers. A consequence of this reality should be that the radius of curvature should be larger since the displacement is in smaller amounts. Hence, this comment is validated in Fig. 15. The figure shows that the radius of curvature is nearly constant till $Ra = 10^3$.

During the iterations between the physics, several undershoots and overshoots are observed as the system tries to reach the steady state. For small *Ra* numbers, the final radius of curvature is decided in less iterations; however, for larger values, more iterations are necessary because of the underdamped solution. This issue is depicted in Fig. 16. This outcome is supported with Fig. 17 where one can observe that

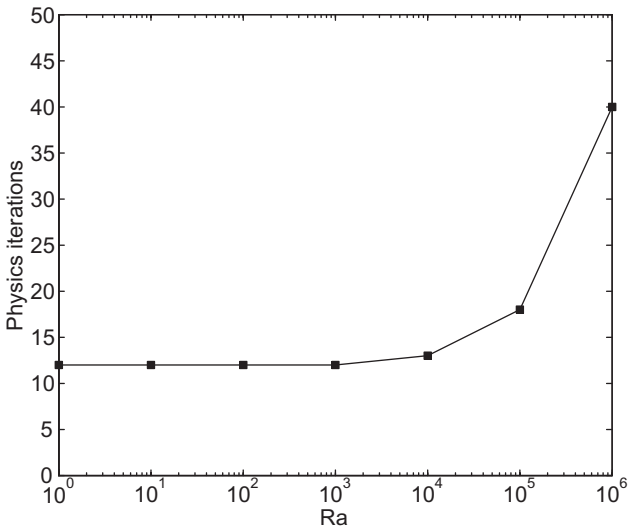

Fig. 17 Iterations between physics

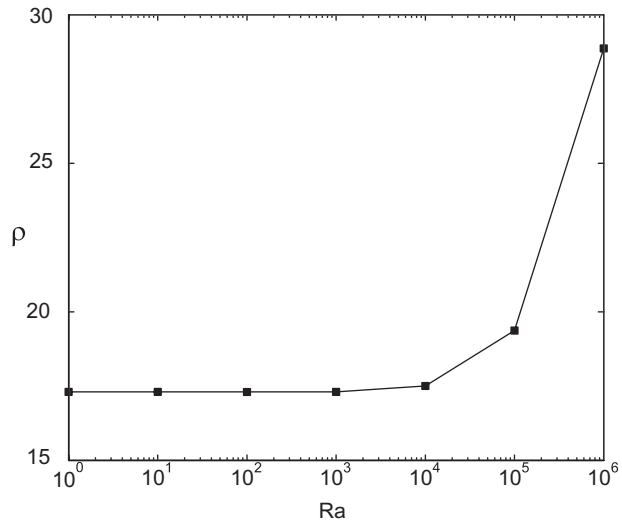

Fig. 15 Radius of curvature

the number of iterations between the fluid and solid increases as *Ra* number increases. Fig. 18 shows the total number of subdomain solves with respect to *Ra* number. Here also the findings are as expected, as convection dominates (with increasing *Ra* number), the problem becomes more non-linear and the number of domain visits increases. In Fig. 19, the convergence of the error in the non-linear least-square problem is presented. For large *Ra* numbers, convergence history suffers from unexpected peaks, but eventually the norm of the error decreases for all *Ra* numbers studied in this work. That means, when a problem is finished, the temperature values as well as the deformation of the slab comes to an end and the curvature is compatible for all elements in the structure. As an extreme case, a temperature scale of 500 is also considered. Computations are held for $Ra = 10^4$ and the plots are

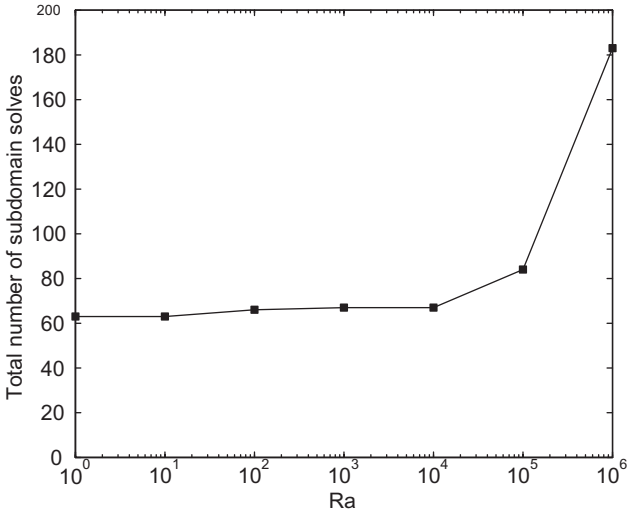

Fig. 18 Total number of visits

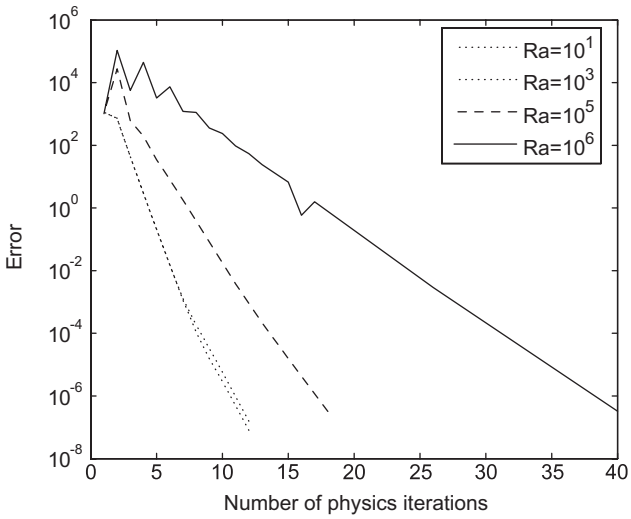

Fig. 19 Convergence of least square

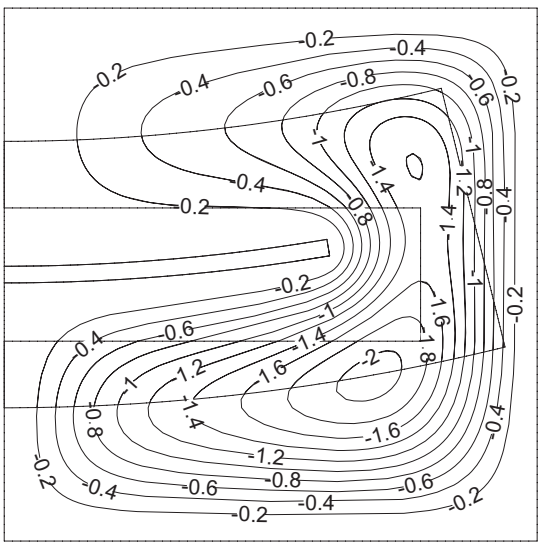

Fig. 20 Stream function contours

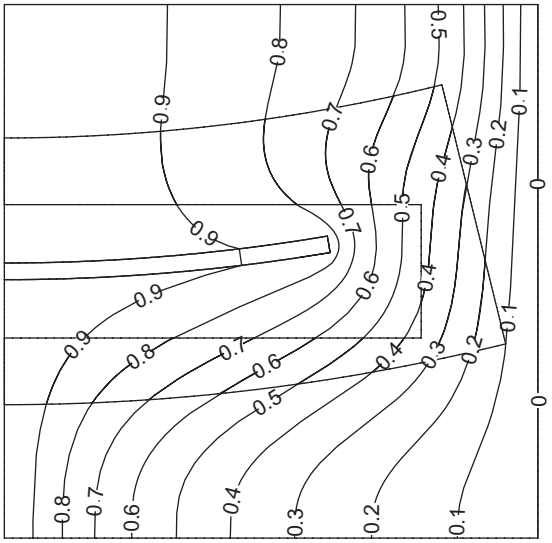

Fig. 21 Temperature distribution

given in Figs 20 and 21. The radius of curvature is calculated as 3.677 and a total of 70 subdomain solves are performed in 11 physics iterations. Compared to the former $Ra = 10^4$ problem, it can be said that less physics iterations are performed; however, the total number of domain visits is increased.

5 CONCLUSIONS

In this study, a fluid–structure problem is investigated such that a flow field around a bimetallic strip is to be found. The strip is allowed to deform. Hence, a strategy based on domain decomposition is used to reflect this change in the geometry into the fluid domain. The flow region is divided into two overlapping subdomains. The outer domain is kept the same and analysed in Cartesian co-ordinates; however, the inner domain is modified such that it is conformable with the deformed strips. The inner domain is studied with polar co-ordinates. The formation of the deflected geometry is based on the computation of the radius of curvature, an average over the deflected elements.

The fluid part is analysed with the stream function–vorticity approach for various Rayleigh numbers and discretized with finite differences. On the contrary, the solid part is examined with plane-strain assumption and solved through finite elements. The coupling between physics is achieved with heat flow. After the solution of the fluid equations, heat fluxes through the inner boundaries of the flow region are calculated. Then a conduction equation, with non-homogeneous Neumann boundary conditions, is solved for the solid part. After the calculation of the temperature field, thermal deformation of the strip is computed. When the fluid domain is visited

again, recently computed temperature values on the solid are implemented as non-homogeneous Dirichlet boundary conditions.

Nonlinear equations are solved with the Newton-GMRES methodology. The matrix-free approach is followed to avoid the formation of the Jacobian matrix. EBE computations are held during the solution of the finite-element equations. The proposed solution algorithm is tested, first for a fixed radius of curvature to show that the solver can handle large changes in the flow domain. In the second part, the calculations are enhanced with the consideration of thermoelasticity. It is observed that the geometry changes when the thermal strains are implemented and the inner domains adapt themselves to the deformed body.

To take the study one step further, one can analyse solids with different properties, like orthotropic for instance. In reality, elastic deformation occurs only in small amounts. In this study, it is shown that the proposed method works well even for small radii of curvature. As a result, problems with large deformations like in plasticity, might also be investigated. Additionally, a transient analysis can be conducted to understand the stability of the structure. In terms of the computational aspects, non-linear preconditioning and multigrid can be employed. Parallel implementations should also be considered to reveal the power of domain decomposition.

ACKNOWLEDGEMENT

This work was supported by Bogazici University Research Fund, grant number BAP 07A601D.

REFERENCES

1 **Fung, Y. C.** *The theory of aeroelasticity*, 1969 (Dover, New York).
2 **Saad, Y.** and **Schultz, M. H.** A generalized minimal residual algorithm for solving nonsymmetric linear systems. *SIAM J. Sci. Stat. Comput.*, 1986, **7**, 856–869.
3 **van der Vorst, H.** Bi cgstab: a fast and smoothly converging variant of BICG for the solution of nonsymmetric linear systems. *SIAM J. Sci. Stat. Comput.*, 1992, **13**, 631–644.
4 **Dembo, R. S., Eisenstat, S. C.,** and **Steihaug, T.** Inexact Newton methods. *SIAM J. Numer. Anal.*, 1982, **19**, 400–408.
5 **Brown, P. N.** and **Saad, Y.** Hybrid Krylov methods for nonlinear-systems of equations. *SIAM J. Sci. Stat. Comput.*, 1990, **11**, 450–481.
6 **Gropp, W., Keyes, D., McInnes, L. C.,** and **Tidriri, M. D.** Globalized Newton–Krylov–Schwarz algorithms and software for parallel implicit CFD. *Int. J. High Perform. Comput. Appl.*, 2000, **14**, 102–136.
7 **Pawlowski, R. P., Shadid, J. N., Simonis, J. P.,** and **Walker, H. F.** Globalization techniques for Newton–Krylov methods and applications to the fully coupled solution of the Navier–Stokes equations. *SIAM Rev.*, 2006, **48**, 700–721.
8 **Timoshenko, S. P.** Analysis of bi-metal thermostats. *J. Opt. Soc. Am.*, 1925, **11**, 233–255.
9 **Boley, B. A.** and **Weiner, J. H.** *Theory of thermal stress*, 1960 (Wiley, New York).
10 **de Vahl Devis, G.** and **Jones, I. P.** Natural convection of air in a square cavity: a comparison exercise. *Int. J. Numer. Methods Fluids*, 1983, **3**, 227–248.
11 **de Vahl Devis, G.** Natural convection of air in a square cavity: a bench mark numerical solution. *Int. J. Numer. Methods Fluids*, 1983, **3**, 249–264.
12 **Lequéré, P.** Accurate solutions to the square thermally driven cavity at high Rayleigh number. *Comput. Fluids*, 1991, **20**, 29–41.
13 **Shi, X.** and **Khodadadi, J. M.** Laminar natural convection heat transfer in a differentially heated square cavity due to a thin fin on the hot wall. *Trans. ASME*, 2003, **125**, 624–634.
14 **Bilgen, E.** Natural convection in cavities with a thin fin on the hot wall. *Int. J. Heat Mass Transf.*, 2005, **48**, 333–390.
15 **Schwarz, H. A.** Ueber einige Abbildungsaufgaben. *Gesammelte Math. Abhandlungen*, 1869, **11**, 65–83.
16 **Bejan, A.** *Convection heat transfer*, 3rd edition, 2004 (Wiley, New Jersey).
17 **Timoshenko, S. P.** and **Goodier, J. N.** *Theory of elasticity*, 3rd edition, 1970 (McGraw-Hill, New York).
18 **Pepper, D. W.** and **Heinrich, J. C.** *The finite element method: basic concepts and applications*, 2nd edition, 2006 (Taylor & Francis, New York).
19 **Cook, R. D.** *Finite element modeling for stress analysis*, 1995 (Wiley, New York).
20 **Fellipa, C. A., Park, K. C.,** and **Farhat, C.** Partitioned analysis of coupled mechanical systems. *Comput. Methods Appl. Mech. Eng.*, 2001, **190**, 3247–3270.
21 **Nicholson, D. W.** *Finite element analysis: thermomechanics of solids*, 2003 (CRC Press, Boca Raton, FL).
22 **Qin, N., Ludlow, D. K.,** and **Shaw, S. T.** A matrix-free preconditioned Newton-GMRES method for unsteady Navier–Stokes solutions. *Int. J. Numer. Methods Fluids*, 2000, **33**, 223–248.
23 **Smith, I. M.** and **Griffiths, D. V.** *Programming the finite element method*, 4th edition, 2004 (Wiley, Hoboken).
24 **Smith, B., Bjorstad, P.,** and **Gropp, W.** *Domain decomposition*, 1996 (Cambridge Publications, Philadelphia).
25 **Strikwerda, J. C.** and **Scarbnick, C. D.** A domain decomposition method for incompressible viscous flow. *SIAM J. Sci. Stat. Comput.*, 1993, **14**, 49–67.
26 **DeWitt, D. P.** and **Incropera, F. P.** *Introduction to heat transfer*, 4th edition, 2001 (Wiley, New York).
27 **Ugural, A. C.** and **Fenster, S. K.** *Advanced strength and applied elasticity*, 3rd edition, 1994 (Prentice Hall, New Jersey).

APPENDIX

Notation

c_p	specific heat
D	stiffness matrix

E	modulus of elasticity
$\boldsymbol{f}$	body force
g	gravity
$\boldsymbol{J}$	Jacobian matrix
k	thermal conductivity
Nu	Nusselt number
Pr	Prandtl number
Ra	Rayleigh number
T	temperature
$\boldsymbol{u}$	velocity vector
u	displacement in x-direction
v	displacement in y-direction
α	thermal diffusivity
α_s	coefficient of thermal expansion of solid
β	coefficient of thermal expansion of fluid
ε	strain
η	forcing factor
μ	dynamic viscosity
ν	kinematic viscosity, Poisson's ratio
ρ	density
σ	stress
ψ	stream function
Ω	vorticity